Gas-Liquid Mass Transfer from a Single Bubble in Liquid-Solid Fluidized Beds

Experiments were conducted to study the gas-liquid mass transfer of a single bubble containing an ozone-oxygen gas mixture in liquids and liquid-solid fluidized beds. A spectrophotometric technique is developed for the measurement of the instantaneous mass transfer coefficient and the local concentration distribution around the bubble wake. The method employs an ultraviolet light source and optical fibers. Axial variations of the mass transfer rate are studied. An ozone and starch-iodide complex reaction is employed to visualize the mass transfer phenomena.

Gyung-Ho Song
Liang-Shih Fan
Department of Chemical Engineering
Ohio State University
Columbus, OH 43210

Introduction

Any physical, chemical, petrochemical, or biochemical operation with mass transfer between gas and liquid phases involves a diffusional step in which the solute is transported either from the gas-liquid interface into the solution or vice versa. In a bubble column, gas-slurry, or gas-liquid-solid fluidized beds, the gas-liquid mass transfer step plays an important role in the performance of the reactor (Fan, 1989). The volumetric gas-liquid mass transfer coefficient for the absorption of a gas phase component into a liquid phase in a gas-liquid-solid fluidized bed has been extensively studied (Ostergaard and Suchozebrski, 1971; Lee and Worthington, 1974; Dakshinamurty et al., 1973, 1974; Dhanuka and Stepanek, 1980a, b; Alvarez-Cuenca and Nerenberg, 1981; Lee and Buckley, 1981; Alvarez-Cuenca et al., 1984; Nguyen-Tien et al., 1985). However, due to the complexities of the system, very little work has been attempted to measure the instantaneous mass transfer coefficient between a bubble and a liquid-solid suspension. To understand the fundamental mechanisms of the gas-liquid mass transfer, one can first examine the mass transfer behavior of a single bubble in a liquid-solid fluidized bed based on the bubble wake mechanics proposed by Tsuchiya and Fan (1986).

Extensive experimental and theoretical studies on the gas-liquid mass transfer of a single bubble in liquids have been reported in the literature. Experimental studies for absorption of gases such as CO_2, acetylene, and sulfur dioxide in water or dilute aqueous solutions have been performed by several investigators (Calderbank and Lochiel, 1964; Davenport et al., 1967; Calderbank et al., 1970; Guthrie and Bradshaw, 1973; Coppus and Rietema, 1980, 1981). Measurement techniques can be classified into two major catagories: the constant pressure method (Baird and Davidson, 1962; Leonard and Houghton, 1963; Davenport et al., 1967; Johnson et al., 1969) and the constant volume method (Calderbank and Lochiel, 1964; Calderbank et al., 1970; Koide et al., 1974, 1976).

Theoretical models for the gas-liquid mass transfer rate in liquid media have been developed by Baird and Davidson (1962), Lochiel and Calderbank (1964), Coppus and Rietema (1980 and 1981), and Jean and Fan (1989). The contributions of the front and the base of a spherical-cap bubble to the total mass transfer rate have been separately studied. The gas-liquid mass transfer rate at the roof of a single spherical-cap bubble was studied by Baird and Davidson (1962), Lochiel and Calderbank (1964), and Coppus and Rietema (1980). The prediction for the mass transfer rate at the base of a single spherical-cap bubble has been also attempted by Calderbank et al. (1970), Brignell (1974), Weber (1975), and Coppus and Rietema (1981).

The effect of the residence time of a single bubble on mass transfer rate was observed by several investigators (Baird and Davidson, 1962; Guthrie and Bradshaw, 1973; Coppus and Rietema, 1981). They found that the mass transfer coefficient initially decreased with increasing residence time of the bubble in liquids and eventually approached an asymptotic value. The reason was mostly attributed to surface effects of surface active agents. The surface flow was found to be retarded by the trace contaminant adsorbed at the gas-liquid interface, which in turn decreased the mass transfer coefficient (Koide et al., 1971). The captive wake of the bubble was also suggested as a cause of the unsteady-state behavior (Baird and Davidson, 1962; Coppus

Correspondence concerning this paper should be addressed to L.-S. Fan.

and Rietema, 1981). On the other hand, several researchers (Calderbank and Lochiel, 1964; Leonard and Houghton, 1963) observed that the unsteady-state behavior was found only for small bubbles. Using the concept of a stagnant region for bubbles and drops, Weber (1975) proposed a model to predict mass transfer coefficients for spherical-cap bubbles influenced by surface active agents.

Most of the investigations on the gas-liquid mass transfer have been confined to the mass transfer in liquid media; little has been done on the mass transfer of a single bubble in liquid-solid fluidized systems. Vanderschuren et al. (1974) measured the volumetric mass transfer coefficient of a large, single spherical-cap gas bubble (carbon dioxide, benzene, or chloroethane) in a three-dimensional liquid-solid fluidized bed containing 450 μm glass beads by sampling and analyzing the gas from the bubble at various heights. Their reported mass transfer coefficients were, however, an average for the part of the column between the bubble injection and the sampling point. Their results indicated that the volumetric mass transfer coefficient initially decreased sharply with axial distance and then leveled off. They also presented an empirical correlation relating the mass transfer coefficient to the system operating variables and the diffusivity of the dissolved gas in liquids. A theoretical treatment of the gas-liquid mass transfer in liquid-solid systems was given by Jean and Fan (1989). In their model, they considered the mass transfer through the bubble roof and through the bubble base as two different mechanisms. They further divided the mass transfer through the bubble base into two cases depending on system operating conditions. They obtained reasonably good predictions for the overall gas-liquid mass transfer coefficient of a single bubble in liquids as well as in liquid-solid fluidized beds.

In this study a spectrophotometric technique, based on a light absorption principle, and a data processing technique are developed for direct measurement of the instantaneous gas-liquid mass transfer coefficient of a single circular-cap bubble in liquids and liquid-solid fluidized beds. Since the resistance over the gas side of the interface is much less than that over the liquid side (Davenport et al., 1967), only the liquid side mass transfer coefficient is considered. Axial variations of the concentration, bubble volume, and the volumetric mass transfer coefficient are studied. In addition, an ozone and starch-iodide complex reaction is employed to visualize the gas-liquid mass transfer phenomena.

Experimental Method

Apparatus

A two-dimensional fluidized bed, shown in Figure 1, was employed. It permitted simultaneous measurement of gas concentration using a UV spectrophotometric probe and visual observation of the bubble wake behavior. The two-dimensional column made of acrylic polymer was 1.4 m high and 0.3 m wide, with 8 mm nominal gap thickness. A porous plate was used as the liquid distributor.

Water and glass beads (460 μm) were used as the liquid and solid phases, respectively. A single large circular-cap gas bubble, controlled by a solenoid valve, was injected into the two-dimensional fluidized bed through a 6.4 mm ID nozzle that was flush-mounted on the front wall, 0.13 m above the liquid distributor. The bubble was an ozone-oxygen mixture with approximately 2 ~ 3 wt. % of ozone gas produced by an ozone generator (Welsbach, Ozonator T-408). Although dissolved ozone reacts with water (Hewes and Davison, 1971), the reaction rate constant is relatively small compared to the mass

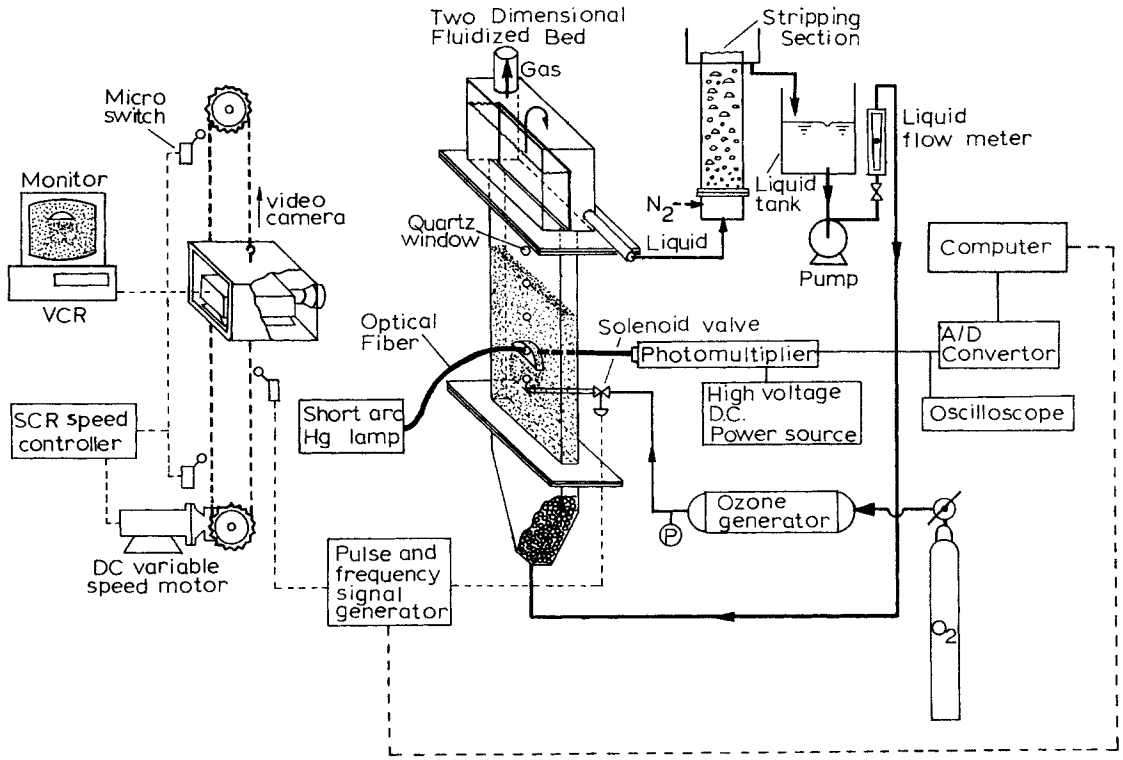

Figure 1. Experimental system.

transfer rate of the ozone estimated from the correlation obtained by Vanderschuren et al. (1974). Hence, the mass transfer rate should not be affected by the slow reaction of water with ozone. In addition, there is no effect of inert gas on a gas-film resistance in the gas-liquid mass transfer of a bubble containing inert and soluble gas mixtures (Danckwerts, 1965; Weller, 1972). Temperatures of the continuous liquid flow and the gas bubble were maintained at 2 ± 1°C in order to increase the mass transfer rate of ozone in the liquid medium. The recycled liquid was maintained free of ozone by degassing with nitrogen in the stripping column. The experimental conditions used in each run are summarized in Table 1.

A 2 mm optical fiber probe (Oriel fused silica cable) similar to that of Kitano and Fan (1988) was mounted on the front wall of the two-dimensional bed. A short arc mercury lamp (Osram, HBO 500 W/2), which had high radiance in the medium and long wavelength UV spectrum, was located in front of the bed and was lit by a DC power source. Seven pairs of quartz windows (ESCO, S1-UV), which allowed the passage of a UV beam and a reference beam, were imbedded at various levels in both sides of the column. The light passing through the fluidized bed was received by a bifurcated optical fiber (Oriel fused silica bifurcated fiber optic cable) which in turn transmitted the light to photomultipliers (Hamamatsu, 1P28 and R166) with two different narrow-band filters (254 and 500 nm Oriel narrow-band interference filter). The photomultipliers were interfaced with two different channels of an analog/digital converter (Metra-Byte, Dash-16) installed in a microcomputer for data analysis and recording. Software was developed for the data processing and storage of 1,000 data points per second for each channel.

The injection of a bubble into the bed was triggered by the pulse signal generator, which was also interfaced with the computer to initiate the data acquisition. After finishing the measurement at a given axial position, the optical fibers were moved to a new level without changing the injection volume of bubbles.

Signal analysis

The ozone concentration inside the gas bubble can be measured based according to the Beer-Lambert law, taking into account particle interference effects on the transmission of the UV and visible wavelengths. To relate the output voltages, as

Table 1. Experimental Conditions

Gas phase:	Ozone (O_3)–oxygen (O_2) mixture (2 ~ 3 wt.% Ozone) Diffusivity of ozone in water: $D = 1.305 \times 10^{-5}$ cm^2/s from Wilke-Chang equation (1955) Henry's law constant (O_3): $H = 2.036 \times 10^3$ atm/mol frac.
Liquid phase:	Tap water (2 ± 1°C) $\rho_L = 0.999$ gm/cm^3 $\sigma_L = 75.53$ dyne/cm $\mu_L = 1.664$ cP
Solid particle:	Glass beads $d_P = 460\ \mu$m $\rho_S = 2.50$ gm/cm^3 $U_t = 6.73$ cm/s
Bed condition:	$\epsilon = 1.0, 0.75, 0.65, 0.55$

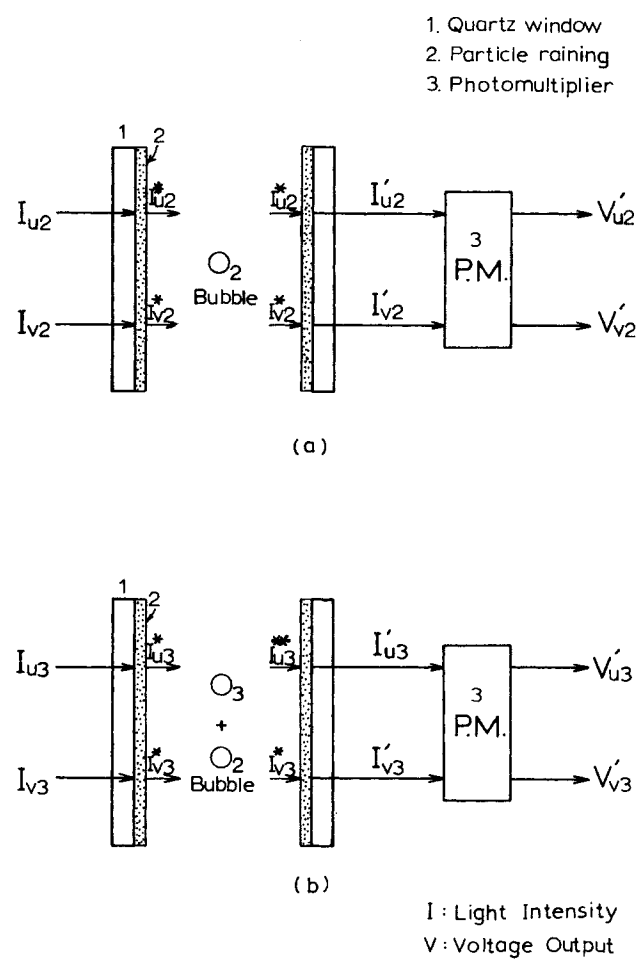

Figure 2. Signal processing.

indicated in Figure 2, to the ozone concentration, the following assumptions are made:

1. The Beer-Lambert law can be applied to I^*_{u3} and I^{**}_{u3}, that is:

$$\log_{10}\left(\frac{I^{**}_{u3}}{I^{*}_{u3}}\right) = -\alpha C \ell \tag{1}$$

where α is the specific absorption coefficient expressed as a base-10 logarithm.

2. The relative reduction of light intensity by the particles for the same wavelength is always the same for systems (a) and (b).

$$\frac{I^*_{u3}}{I_{u3}} = \frac{I^*_{u2}}{I_{u2}}, \frac{I'_{u3}}{I^{**}_{u3}} = \frac{I'_{u2}}{I^*_{u2}} \tag{2a}$$

$$\frac{I^*_{v3}}{I_{v3}} = \frac{I^*_{v2}}{I_{v2}}, \frac{I'_{v3}}{I^*_{v3}} = \frac{I'_{v2}}{I^*_{v2}} \tag{2b}$$

3. The relationship between the light intensity and the voltage output from the photomultipliers is linear, that is:

$$V'_{u3} = \beta_u I'_{u3}, \quad V'_{u2} = \beta_u I'_{u2},$$

$$V'_{v3} = \beta_v I'_{v3}, \quad V'_{v2} = \beta_v I'_{v2} \tag{3}$$

where β_u and β_v are conversion factors of the photomultipliers. Since particle interference effects on the transmission of the UV and the visible wavelengths are different, we have

$$\left(\frac{I^*_{u3}}{I_{u3}}\right) = \lambda_1 \left(\frac{I^*_{v3}}{I_{v3}}\right) \quad \text{and} \quad \left(\frac{I'_{u3}}{I^{**}_{u3}}\right) = \lambda_2 \left(\frac{I'_{v3}}{I^*_{v3}}\right) \tag{4}$$

Note that the proportionality constants, λ_1 and λ_2, are unity for pure liquid media since there is no particle effect. Substitution of I^*_{u3} and I^{**}_{u3} by Eq. 4 into Eq. 1 yields

$$\log_{10}\left(\frac{1}{\eta\lambda}\right)\left(\frac{I'_{u3}}{I'_{v3}}\right) = -\alpha C \ell \tag{5}$$

where $\lambda = \lambda_1 \lambda_2$ and $\eta = (I_{u3}/I_{v3}) = (I_{u2}/I_{v2})$.

Combination of Eqs. 3 and 5 gives

$$\log_{10}\left(\frac{V'_{v3}}{V'_{u3}}\right) = \alpha C \ell + \log_{10}\left(\frac{\beta_v}{\beta_u}\frac{1}{\eta\lambda}\right) \tag{6}$$

and, in the case of bubble rise in pure liquid, λ is unity. From Eqs. 2–4, λ can be expressed as

$$\lambda = \lambda_1 \lambda_2 = \frac{I_{v2}}{I'_{v2}}\frac{I'_{u2}}{I_{u2}} = \frac{\beta_v}{\eta\beta_u}\frac{V'_{u2}}{V'_{v2}} \tag{7}$$

Combining Eqs. 6 and 7 results in

$$\log_{10}\left(\frac{V'_{v3}}{V'_{u3}}\right) = \alpha C \ell + \log_{10}\left(\frac{V'_{v2}}{V'_{u2}}\right) \tag{8}$$

From Eq. 6, $\alpha\ell$ can be determined by the slope of the semilog plot of V'_{v3}/V'_{u3} vs. the concentration of the standard solution of potassium chromate (K_2CrO_4) in the fluidized bed. Knowing α of potassium chromate (2,776.5 $mol^{-1} \cdot cm^2$ at 255 nm; Mellon, 1950), ℓ is evaluated from the slope, $\alpha\ell$, to be 0.07 cm. Note that the specific absorption coefficient at 254 nm for ozone is expressed in terms of pressure unit in the literature (e.g., $\alpha = 130$ $atm^{-1} \cdot cm^{-1}$ at 254 nm; Horvath et al., 1985). In order to evaluate the ozone concentration by means of Eqs. 6 and 8, concentration is expressed in terms of partial pressure, p_A. A similar but less rigorous calibration scheme for the measurement of ozone concentration in a gas bubble in gas-solid fluidized beds can be found in Furusaki and Akagi (1983).

Estimation of bubble volume

Even though the two-dimensional nature of the fluidized bed enables bubble size, velocity, and shape to be measured rather easily, the actual shape of the bubbles is not completely two-dimensional and the front of the bubbles is round-nosed because of the side wall effect. Therefore, the bubble shape is considered as shown in Figure 3. It can be shown from geometry that the lower portion of the bubble volume is given by

$$V_1 = w\{[R^2\theta_m - \tfrac{1}{2}b(R-h)] - [R^2\theta' - \tfrac{1}{2}b'(R-h_1)]\} \tag{9a}$$

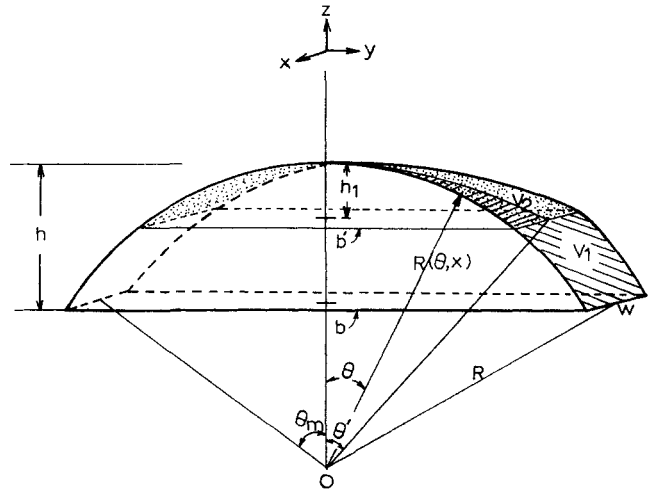

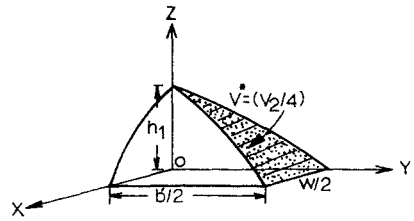

Figure 3. Bubble shape in a two-dimensional fluidized bed.

The upper portion of the bubble volume, V_2, is obtained by

$$V_2 = 2R^2 w\left\{\frac{R}{2h_1}\left[\frac{\pi}{2} - \phi \sin^{-1}\phi - \sqrt{1-\phi^2}\right] + \frac{R}{6h}(1-\phi^2)^{3/2} - \left(\frac{1}{2}\right)[\sin^{-1}\phi + \phi\sqrt{1-\phi^2}]\right\} \tag{9b}$$

where:

$$\phi = (1 - h_1/R); \quad h = h_1 + h_2$$

$$\theta_m = 2\tan^{-1}(2/E); \quad \theta' = \cos^{-1}(1 - h_1/R)$$

$$E = b/h; \quad R = (h/8)(E^2 + 4)$$

$$b' = 2R\sin\theta'$$

As a consequence, total volume can be expressed as

$$V_B = V_1 + V_2 \tag{10}$$

Instantaneous gas-liquid mass transfer coefficient

In order to evaluate the mass transfer coefficient during the rise of the bubble, determinations of concentration variation (dC_A/dt) and the bubble volume change with time (dV_B/dt) are

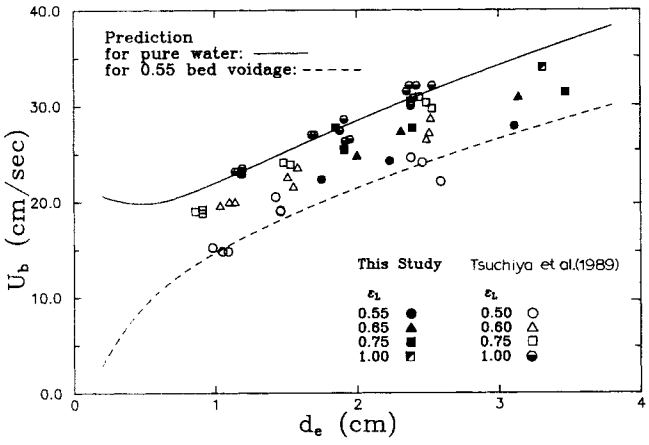

Figure 4. Bubble rise velocity and bubble size for various bed expansions.

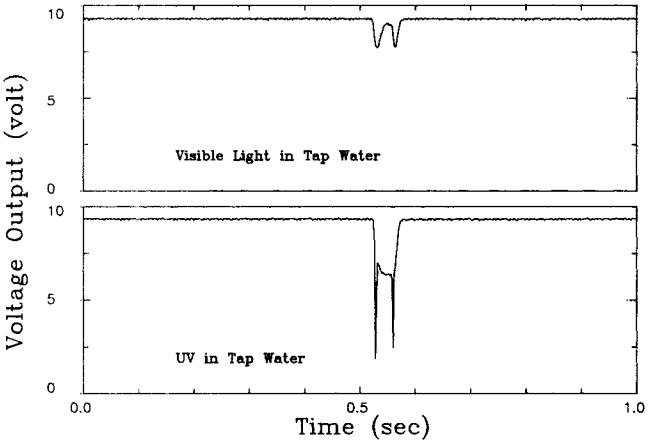

Figure 5a. Probe signals along bubble wake center in a liquid medium.

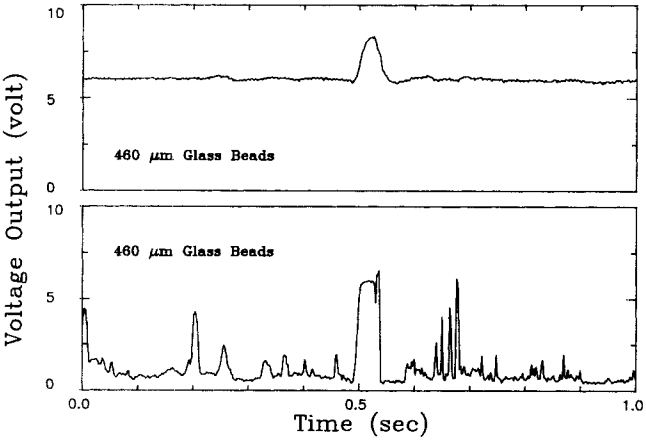

Figure 5b. Probe signals along bubble wake center in a liquid-solid fluidized bed.

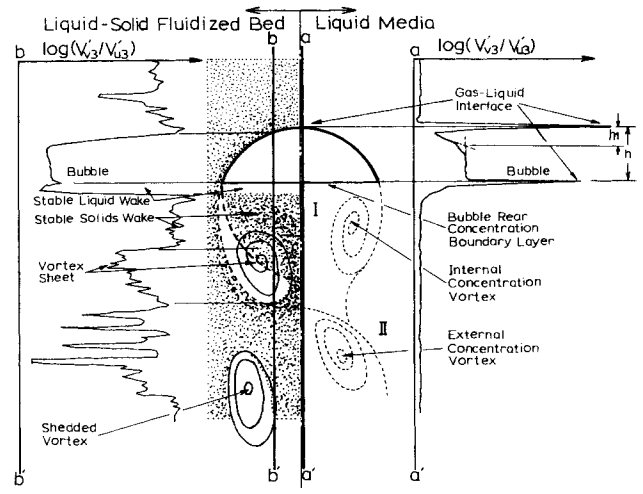

Figure 6. Local concentration distribution in bubble wake.

needed. Assuming that ozone is an ideal gas, the ideal gas law can be used to convert the partial pressure, p_A, to the molar concentration, C_A (gmol/cm^3):

$$C_A = \frac{p_A}{R'T} \tag{11}$$

where R' is the universal gas constant (82.05, cm^3 · atm/gmol · K), T is the temperature in K, and p_A is the partial pressure of ozone gas in atm.

The saturated ozone concentration, C_A^*, at the gas-water interface can be obtained from Henry's law:

$$p_A = H x_A^* = H\left(\frac{18C_A^*}{1 - 30C_A^*}\right) \tag{12}$$

where H is the Henry's law constant (atm/mol frac.) and x_A^* is the mole fraction of the dissolved ozone in water.

Therefore, the volumetric gas-liquid mass transfer coefficient,

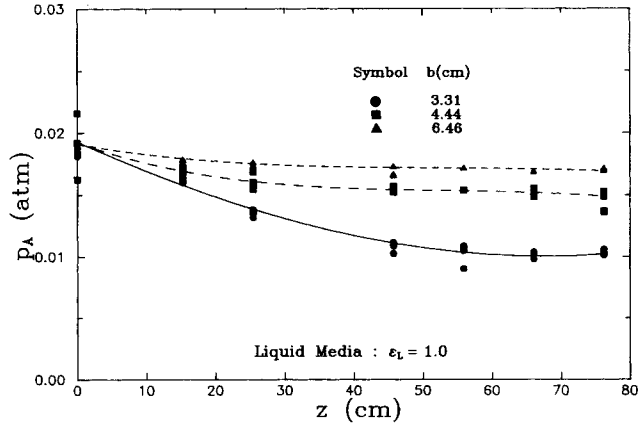

Figure 7. Axial variation of partial pressure of ozone in a liquid medium.

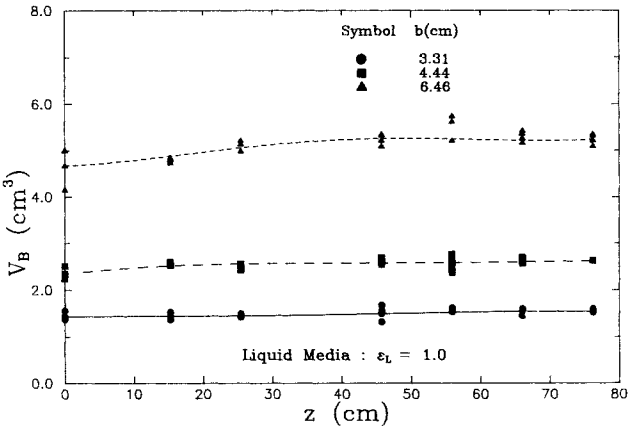

Figure 8. Axial variation of bubble volume in a liquid medium.

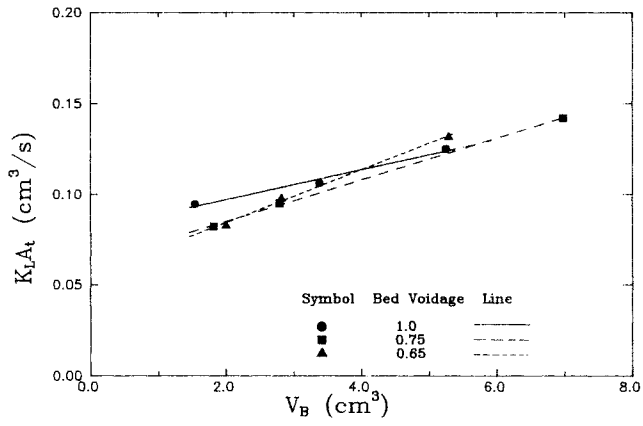

Figure 10. Volumetric gas-liquid mass transfer coefficient as a function of bubble volume.

K_LA_t, is calculated by

$$K_L A_t = \frac{-\Delta n_A/\Delta t}{C_A^* - C_{Ab}} \tag{13}$$

where $\Delta n_A = \Delta(C_A V_B)$ and $\Delta t = \Delta z/U_B$, and Δn_A is the difference in the number of moles of ozone and Δz is the difference in height between the positions of the neighboring pairs of quartz windows. U_B is the absolute bubble rising velocity. C_{Ab}, the bulk ozone concentration in the liquid-solid suspension, is assumed to be zero.

Results and Discussion

Bubble rise velocity

The mass transfer rate between the bubble and the liquid is influenced by hydrodynamic conditions of the bubble such as the bubble rise velocity and the bubble shape. The bubble rise velocities for various bed expansions are plotted against the bubble size in Figure 4. Note that, due to a decrease in the hydrostatic head and an unsteady-state bubble formation, the bubble expands as it rises in the column and, as a consequence, the rise velocity is not constant along the axial direction. Therefore, the reported bubble rise velocity and the particular bubble size are averages from several locations. Figure 4 shows that the bubble rise velocity increases with increasing bubble size and bed expansion. The rise velocities of the bubbles in water are always larger than those in a liquid-solid fluidized medium. In Figure 4, experimental results for the rise velocity of ozone-oxygen mixture bubbles in this study are compared with the bubble rise velocities of pure nitrogen bubbles and the semiempirical equation for the bubble rise velocity reported by Tsuchiya et al. (1989).

At the same hydrodynamic conditions the deviations of the bubble rise velocities of ozone-oxygen mixture bubbles from those of pure nitrogen bubbles are negligible and the prediction agrees fairly well with the bubble rise velocities in pure liquids and liquid-solid fluidized beds. Therefore, the rise velocity of ozone-oxygen mixture bubbles is not affected by mass transfer

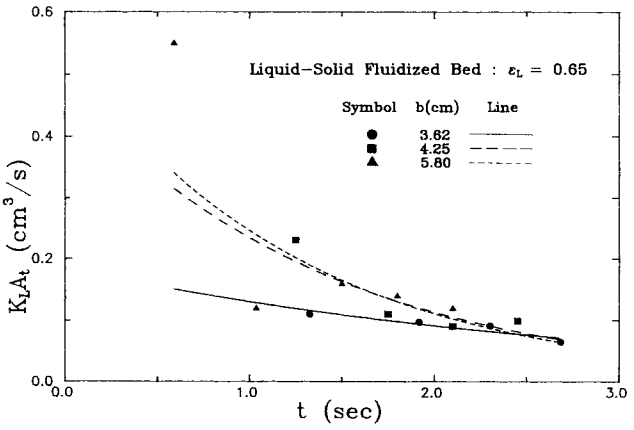

Figure 9. Axial variation of volumetric gas-liquid mass transfer coefficient in a liquid-solid fluidized bed.

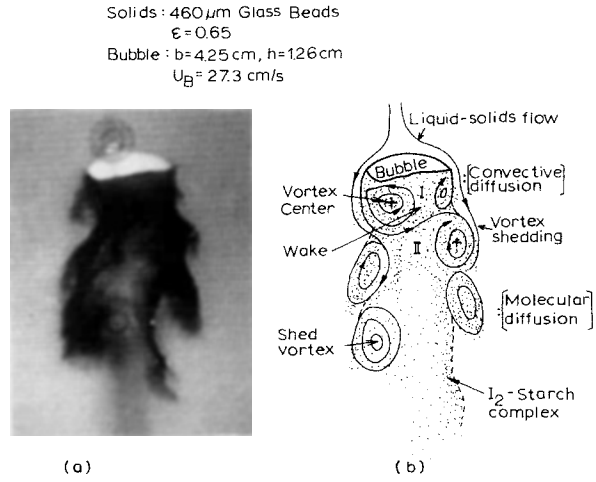

(a) Photograph
(b) Interpretation of the gas-liquid mass transfer.

Figure 11. Circular-cap ozone-oxygen bubble and its wake rising through a starch-iodide-water and 460 μm glass bead fluidized bed.

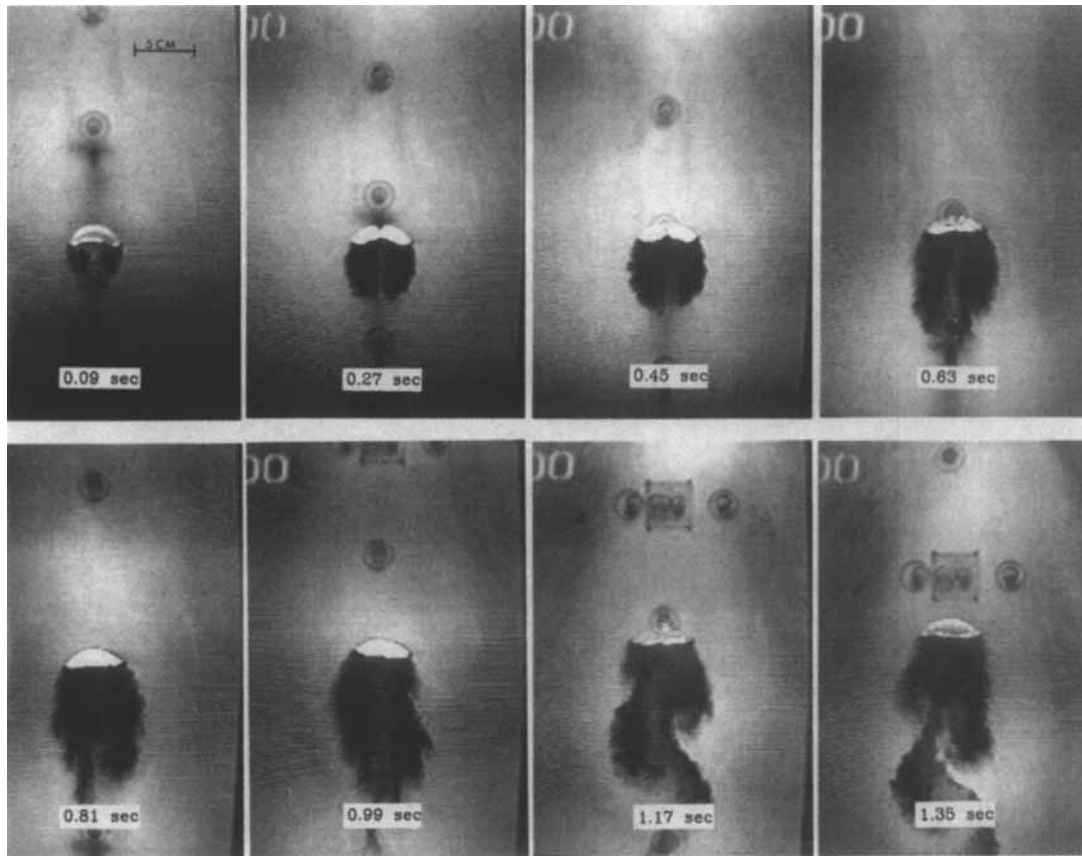

Figure 12a. Circular-cap ozone-oxygen bubble and its wake rising in a stationary starch-iodide-water medium.

since the rate of change in momentum induced by mass transfer is small in comparison with the rate of change in actual momentum associated with the bubble motion (Davenport et al., 1967).

Local concentration distribution

Figures 5a and 5b show typical probe signals for a single bubble in a liquid medium and in a liquid-solid fluidized bed, respectively. When the bubble containing a mixture of ozone and oxygen crosses the view of the probe, the UV energy (254 nm) is absorbed, but the visible light (500 nm) is not. It is observed that when the probe is within the bubble, the voltage signal is almost uniform, but sharp peaks are found at the interface. The peaks include the wavelength absorption at the roof and the base of the bubble as well as the deflection due to the bubble-liquid interface rippling. Since the Peclet number is large in these systems, the penetration depth in the solvent around the bubble is small so that only thin concentration boundary layers are formed (Brignell, 1974).

In liquid-solid fluidized beds, the near wake is subdivided into four different regions (Kitano and Fan, 1988):

1. A stable liquid wake region
2. A stable solid wake region
3. A vortex sheet region
4. A fluctuating solids wake region

These are clearly observed in the signals in Figure 6. Taking a log ratio of the UV and the visible light signals, the signals are corrected for the particle interference. Figure 6 shows the qualitative concentration distribution around the bubble in terms of log (V'_{v3}/V'_{u3}), which is proportional to the concentration of solute as indicated in Eqs. 6 and 8.

In the liquid medium, the saturation concentration of dissolved ozone is very large at the roof and the base of the bubble; however, the concentration in the bulk region is small, justifying the assumption of zero bulk concentration. Note that the local concentration is not reliable for the solid wake region in the liquid-solid fluidized bed because of severe particle interference. On the other hand, the stable liquid wake and the stable solid wake underneath the bubble base are clearly observed in the signals. It is also seen in Figure 6 that the concentration increases and becomes constant within the bubble. This is attributed to the fact that the bubble has a round nose as shown in Figure 3. Therefore, from Figures 3 and 6, h_1 and h can be estimated so that the bubble volume can be determined in Eqs. 9a–10.

Axial variations of concentration and bubble volume

Typical profiles of the concentration variation with axial distance are presented in Figure 7 for different bubble sizes in the liquid medium. Due to the unsteady-state bubble growth, the ozone concentration drops initially at the bottom of the bed and levels off near the top of the bed. Therefore, a larger part of the mass transfer takes place during the formation of bubbles. It

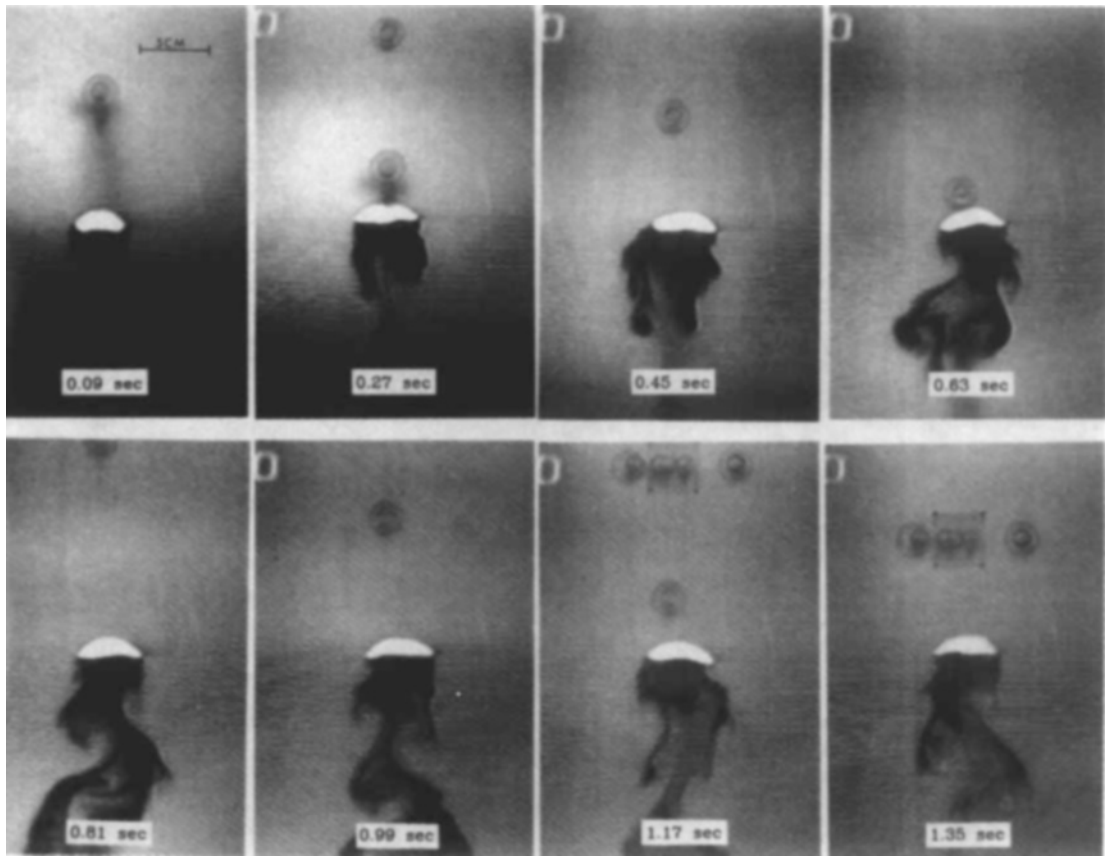

Figure 12b. Circular-cap ozone-oxygen bubble and its wake rising through a starch-iodide-water and 460 μm glass bead fluidized bed, 0.65 bed voidage.

is also observed that the concentration of a small bubble decreases more drastically than that of a large bubble. This can be explained by the difference in the mass transfer rate for different bubble sizes.

The bubble volume is also measured at different axial distances. A typical vertical variation of the bubble volume along the bed is shown in Figure 8. The bubble volume gradually increases as the bubble rises through the bed. There are two counteracting effects on the bubble size variation: hydrostatic pressure and gas mass transfer to the liquid phase. Since only $2 \sim 3$ wt. % of ozone is present in the gas mixture with oxygen and the dissolution of oxygen in water is negligible over the short period of time (2–3 s), the hydrostatic pressure dominates the contribution to the bubble volume change. As a consequence, the variation of bubble volume containing the mixture of ozone and ozygen has the opposite trend compared to the case of highly soluble gases such as carbon dioxide and acetylene, where the bubble volume decreases as the bubble rises.

Volumetric gas-liquid mass transfer coefficient

Since high Peclet number implies that the convective diffusion is dominant as compared to the molecular diffusion through the liquid, the mass transfer is strongly dependent on the bubble-wake motion. In Figure 9 the instantaneous mass transfer coefficients, $K_L A_t$, are plotted against time for different bubble sizes in the liquid-solid fluidized bed. $K_L A_t$ decreases at the bottom of the bed and levels off at the top of the bed. There are several coupling effects for this phenomenon. In tap water, there are trace amounts of surface active materials that are responsible for the reduction of the mass transfer coefficient (Baird and Davidson, 1962; Guthrie and Bradshaw, 1973; Coppus and Rietema, 1981). The mass transfer is retarded by the trace contaminants adsorbed at the gas-liquid interface. More specifically, a slowly moving film of surfactant is supposed to deposit at the bubble surface and in turn reduces mass transfer rate (Guthrie and Bradshaw, 1973; Davenport et al., 1967). In this experiment, however, the unsteady-state bubble formation has a more significant effect. At the bottom of the bed, the mass transfer is strongly affected by the unsteady-state bubble formation associated with the growth of wakes underneath the bubbles and the vortex shedding from the wake to the emulsion phase. Due to the decrease in the hydrostatic pressure and consequent increase in bubble volume, the bubble accelerates continuously as it rises through the liquid. However, these effects become negligible above a certain distance and as a result the bubble rises steadily. At the steady rise of the bubble, the mass transfer coefficient becomes constant.

The volumetric mass transfer coefficient, $K_L A_t$, is shown as a function of bubble volume for different bed voidages in Figure 10. $K_L A_t$ increases with an increase of the bubble volume since A_t increases with increasing bubble size and K_L is relatively insensitive to the bubble size (Calderbank et al., 1970; Jean and Fan, 1989). The mass transfer coefficients obtained from the measurements of ozone gas bubble absorption into water have

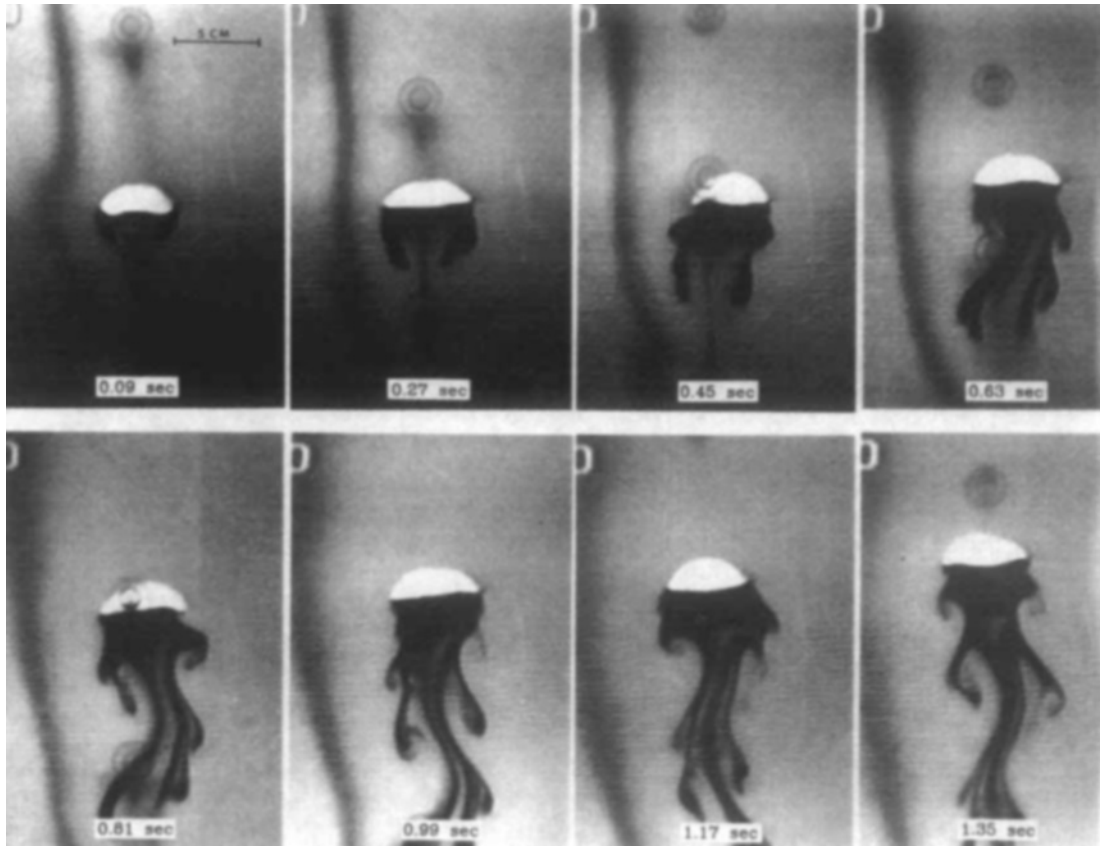

Figure 12c. Circular-cap ozone-oxygen bubble and its wake rising through a starch-iodide-water and 460 μm glass bead fluidized bed, 0.55 bed voidage.

the same trends as the data reported in literature (Vanderschuren et al., 1974).

Visualization of mass transfer phenomena between bubble wakes and bulk phase

In order to visualize the mass transfer phenomena between bubble wakes and bulk flow, the reaction of starch-potassium iodide and ozone molecules is employed as below:

Gas-Liquid Surface

Gas Phase	Liquid Phase				
$\begin{Bmatrix} O_3 \\ O_2 \end{Bmatrix}$	$\rightarrow$	$\begin{Bmatrix} O_3 \\ KI \\ H_2O \end{Bmatrix}$	(A) $\longrightarrow$	$\begin{Bmatrix} I_2 \\ n(C_6H_{10}O_5)_m \end{Bmatrix}$	(B) $\longleftrightarrow$ I_2 = Starch

(A) $O_3 + 2KI + H_2O \rightarrow 2\,KOH + I_2 + O_2$
(B) $I_2 + n(C_6H_{10}O_5)_m \leftrightarrow I_2\text{–}n(C_6H_{10}O_5)_m$

The ozone molecules become visible as a result of the violet color of the iodine-starch complex. Since both reactions (A) and (B) are spontaneous, this technique successfully visualizes the mass transfer patterns of ozone molecules neglecting the reaction step. Detailed description is given elsewhere (Yabe and Kunii, 1978). In Figure 11, the shape and characteristics of the wakes trailing behind the circular-cap bubble present a visual description of the transfer of ozone molecules from the enclosed wake to the bulk liquid by the vortex shedding motion in the column.

The mass transfer of gas bubbles is strongly influenced by the bubble and wake flow behavior. The solute is carried by the flow on the roof of the bubble along the boundary of the wake and is separated into two regions, the wake region, I in Figure 11, by the wake vortex and the liquid-solid fluidized region, II, by the shedding vortex, as shown in Figure 6. The solute that flows into the wake is carried back to the bubble base—the bubble rear concentration boundary layer—and eventually forms an internal concentration vortex (Brignell, 1974). The shed vortex carrying the solute generates an external concentration vortex and eventually diffuses into the bulk flow. In addition to the convective diffusion by the liquid-solid flow, there is slow molecular diffusion of solute from the vortex sheet into the vortex center in the wake and from the surface of wake into the bulk flow, but these contributions are negligible compared to the convective diffusion.

The variations of the mass transfer patterns around the bubbles with respect to time for different bed expansions are shown in Figures 12a–12c. and Table 2. When injected, the initial shape of the bubble is spherical and rapidly changes its shape to a circular cap. As the bubble begins to rise, the reacted ozone molecules are carried from the edge of the bubble by the vortex sheet, and the wake underneath the circular-cap bubble is gradually saturated with the molecules. It is seen that the shape of the bubble plus the wake is approximately circular. The

Table 2. Bubble Characteristics for Various Bed Expansions

Type of Medium	b cm	h cm	E	A_t cm^2	V_B cm^3	U_b cm/s	Re_b
Water	3.31	1.04	3.23	4.91	1.54	27.71	5,504
	4.44	1.28	3.45	6.73	3.38	30.48	8,121
	6.46	1.70	3.85	9.78	5.25	34.00	13,130
$\epsilon = 0.75$	3.45	1.07	3.23	5.45	1.81	25.41	5,737
	4.44	1.29	3.45	6.59	2.80	27.70	7,993
	6.06	1.99	3.03	9.87	6.98	31.40	12,255
$\epsilon = 0.65$	3.62	1.10	3.33	5.55	2.00	24.83	5,757
	4.25	1.26	3.33	6.71	2.82	27.36	7,473
	5.80	1.70	3.33	9.14	5.29	30.93	11,695
$\epsilon = 0.55$	3.16	0.97	3.23	4.69	1.46	22.32	4,447
	4.01	1.24	3.23	5.94	2.31	24.27	6,112
	5.59	1.73	3.23	8.69	5.22	27.90	9,738

zigzag trail behind the bubble is formed in the bulk of the liquid phase as a result of the vortex shedding. It is interesting to note that there is no trace of ozone molecule on the surface of the bubble roof since the reacted molecules are swept by the liquid-solid flow. As a consequence, the convective diffusion induced by potential flow plays an important role in the mass transfer mechanism on the bubble roof. As the bubble rises further, the wake filled completely with gas molecules starts to shed vortices. As shown in Figure 12a, in the liquid medium the parallel vortex shedding mode is first observed at the bottom of the bed and changes to the alternate shedding mode above a certain distance. On the other hand, only alternate sheddings are observed in low bed expansion conditions of the liquid-solid fluidized media, as shown in Figures 12b and 12c. The shed vortices elongate their shape and the gas molecules begin to diffuse out from the center of the vortices into the bulk liquid by molecular diffusion, especially in the case of high bed expansion. In Figure 12c it is seen that the elongated vortices maintain their shape all the way from the bottom to the top of the bed, which implies that the molecular diffusion from the vortices to the liquid-solid fluidized media is negligible for low bed expansion. It is also interesting to note that the vortex motion and the vortex shedding motion in water and high bed expansion systems are highly turbulent. Therefore, it is concluded that the mass transfer from the wakes to the surrounding liquid-solid fluidized media in the high bed expansion systems is larger than that in the low bed expansion systems.

Conclusions

The local concentration distribution and the axial variation of concentration of a single bubble in a liquid and liquid-solid fluidized bed are successfully measured by a UV absorption optical probe. The mass transfer coefficient decreases substantially with the bubble rise at the bottom of the bed and becomes constant near the top of the bed. This behavior is attributed to the unsteady-state bubble formation and vortex shedding at the bottom of the bed. The volumetric mass transfer coefficient increases with increasing bubble volume since the interfacial area, A_t, increases with an increase in the bubble size and the mass transfer coefficient, K_L, is relatively insensitive to the bubble size. With the aid of the reaction of the ozone with starch-iodide complex, the mass transfer patterns for different hydrodynamic conditions are made clearly visible. The mass transfer patterns are highly dependent on the bubble-wake motion.

Acknowledgment

This work is supported by the National Science Foundation, Grant No. CBT-8516874.

Notation

A_t = total surface area of a circular-cap bubble, cm^2
b = bubble breadth, major axis of a spherical-cap or circular-cap bubble, cm
b' = base of upper portion of a bubble in Figure 3, cm
C = solute concentration, mol/cm^3
C_A = concentration of solute (dissolved gas) in solvent, mol/cm^3
C_{Ab} = bulk concentration of solute in solvent, mol/cm^3
C_A^* = concentration of saturated solute in solvent, mol/cm^3
D = molecular diffusivity of dissolved species in liquids, cm^2/s
d_e = bubble size, cm
d_P = particle diameter, cm
E = eccentricity, b/h
h = bubble height, minor axis for a spherical-cap or circular-cap bubble, cm
h_1 = height of upper portion of a bubble in Figure 3, cm
H = Henry's law constant, atm/mol frac
I_{u2} = intensity of ultraviolet energy in an ozone-free bubble system
I_{u3} = intensity of ultraviolet energy in an ozone-containing bubble system
I_{v2} = intensity of visible light in an ozone-free bubble system
I_{v3} = intensity of visible light in an ozone-containing bubble system
K_L = interfacial gas-liquid mass transfer coefficient of a single bubble, cm/s
n_A = number of moles of solute, mol
p_A = partial pressure of ozone gas in an ozone-oxygen mixture, atm
R = radius of curvature for a circular-cap or spherical-cap bubble, cm
R' = universal gas constant, cm^3 · atm/gmol · K
Re_b = bubble Reynolds number based on bubble breadth, bU_b/ν_L
t = time variable, s
T = temperature, K
U_b = bubble rise velocity relative to liquid phase, cm/s
U_B = bubble rise velocity relative to column, cm/s
U_t = particle terminal velocity, cm/s
V_1 = lower portion volume of a circular-cap bubble in Figure 3, cm^3
V_2 = upper portion volume of a circular-cap bubble in Figure 3, cm^3
V_B = bubble volume, cm^3
V'_{u2} = voltage output of ultraviolet energy in an ozone-free bubble system, volt
V'_{u3} = voltage output of ultraviolet energy in an ozone-containing bubble system, volt
V'_{v2} = voltage ouptut of visible light in an ozone-free bubble system, volt

V'_{v3} = voltage output of visible light in an ozone-containing bubble system, volt
w = width of two-dimensional column, cm
x_A^* = mole fraction of saturated solute in solvent
z = axial distance, cm

Greek letters

α = specific absorption coefficient, Eq. 1, $mol^{-1} \cdot cm^2$
β = conversion factor of photomultipliers, Eq. 3
ϵ = holdup
ϵ_L = liquid holdup
ϵ_S = solid holdup
η = ratio of incident energy intensity of 254 and 500 nm
θ = θ-component of spherical coordinates, deg
θ_m = half of the included angle of a spherical-cap bubble, deg
θ' = half of the included angle of upper portion of a bubble in Figure 3, deg
ℓ = cell path length, cm
λ = product of proportionality constants, $\lambda_1\lambda_2$
λ_1, λ_2 = proportionality constants, Eq. 4
μ_L = liquid viscosity, P
ν_L = liquid kinematic viscosity, cm^2/s
ρ_L = liquid density, g/cm^3
ρ_S = solid particle density, g/cm^3
σ_L = liquid surface tension, dyne/cm
ϕ = geometric parameter, $1 - (h_1/R)$

Literature Cited

Alvarez-Cuenca, M., and M. A. Nerenberg, "The Plug Flow Model for Mass Transfer in Three-Phase Fluidized Beds and Bubble Columns," *Can. J. Chem. Eng.*, **59,** 739 (1981).

Alvarez-Cuenca, M., M. A. Nerenberg, and A.-F. A. Asfour, "Mass Transfer Effects Near the Distributor of Three-Phase Fluidized Beds," *Ind. Eng. Chem. Fund.*, **23,** 381 (1984).

Baird, H. I., and J. F. Davidson, "Gas Absorption by Large Rising Bubbles," *Chem. Eng. Sci.*, **17,** 87 (1962).

Brignell, A. S., "Mass Transfer from a Spherical Cap Bubble in Laminar Flow," *Chem. Eng. Sci.*, **29,** 135 (1974).

Calderbank, P. H., and A. C. Lochiel, "Mass Transfer Coefficients, Velocities, and Shapes of Carbon Dioxide Bubbles in Free Rise through Distilled Water," *Chem. Eng. Sci.*, **19,** 485 (1964).

Calderbank, P. H., D. S. L. Johnson, and J. London, "Mechanics and Mass Transfer of Single Bubbles in Free Rise through Some Newtonian and Non-Newtonian Liquids," *Chem. Eng. Sci.*, **25,** 235 (1970).

Coppus, J. H. C., and K. Rietema, "Theoretical Derivation of the Mass Transfer Coefficient at the Front of a Spherical-Cap Bubble," *Chem. Eng. Sci.*, **35,** 1497 (1980).

———, "Mass Transfer from Spherical-Cap Bubbles, the Contribution of the Bubble Rear," *Trans. Inst. Chem. Engrs.*, **59,** 54 (1981).

Dakshinamurty, P., C. Chiranveji, and P. Kameswara Rao, "Studies of Gas-Liquid Mass Transfer in Gas-Liquid Fluidized Beds," *Fluidization and Its Applications,* H. Angelino et al., eds., Cepadues, Toulouse, 429 (1973).

Dakshinamurty, P., P. Kameswara Rao, and K. Veerabhadra Rao, *Indian J. Technol.*, **12,** 276 (1974).

Danckwerts, P. V., "Absorption from Bubbles of Dilute Gas," *Chem. Eng. Sci.*, **20,** 785 (1965).

Davenport, W. G., F. D. Richardson, and A. V. Bradshaw, "Spherical-Cap Bubbles in Low-Density Liquids," *Chem. Eng. Sci.*, **22,** 1221 (1967).

Dhanuka, V. R., and J. B. Stepanek, "Gas-Liquid Mass Transfer in a Three-Phase Fluidized Bed," *Fluidization,* G. R. Grace and G. M. Matsen, eds., Plenum Press, 261 (1980a).

———, "Simultaneous Measurement of Interfacial Area and Mass Transfer Coefficient in Three-Phase Fluidized Beds," *AIChE J.*, **26,** 1029 (1980b).

Fan, L.-S., *Gas-Liquid-Solid Fluidization Engineering,* Butterworth, Stoneham, MA (1989).

Furusaki, S., and H. Akagi, "Direct Measurement of Concentration in Bubbles to Investigate Gas-Solid Contact in Fluidized Beds," *Proc. 4th Int. Conf. on Fluidization,* D. Kunii and R. Toei, eds., Kashikojima, Japan, 549 (1983).

Guthrie, I. L., and A. V. Bradshaw, "Spherical Capped Gas Bubbles Rising in Aqueous Media," *Chem. Eng. Sci.*, **28,** 191 (1973).

Hewes, C. G., and R. R. Davison, "Kinetics of Ozone Decomposition and Reaction with Organics in Water," *AIChE J.*, **17,** 141 (1971).

Horvath M., L. Bilitzky, and J. Huttner, *Ozone,* Elsevier, New York (1985).

Jean, R. H., and L.-S. Fan, "Rise Velocity and Gas-Liquid Mass Transfer of a Single Large Bubble in Liquids and Liquid-Solid Fluidized Beds," *Chem. Eng. Sci.* (1989).

Johnson, A. I., F. Besik, and A. E. Hamilec, "Mass Transfer from a Single Rising Bubble," *Can. J. Chem. Eng.*, **47,** 559 (1969).

Kitano, K., and L.-S. Fan, "Near-Wake Structure of a Single Gas Bubble in a Two-Dimensional Liquid-Solid Fluidized Bed: Solids Holdup," *Chem. Eng. Sci.*, **43,** 1355 (1988).

Koide, K., Y. Orito, and Y. Hara, "Mass Transfer from Single Bubbles in Newtonian Liquids," *Chem. Eng. Sci.*, **29,** 417 (1974).

Koide, K., T. Hayashi, K. Sumino, and S. Iwamoto, "Mass Transfer from Single Bubbles in Aqueous Solutions of Surfactants," *Chem. Eng. Sci.*, **31,** 936 (1976).

Lee, J. C., and P. S. Buckley, in *Biological Fluidized Bed Treatment of Water and Wastewater,* P. F. Cooper and B. Atkinson, eds., Ellis Horwood, England, ch. 4, p. 62 (1981).

Lee, J. C., and H. Worthington, "Gas-Liquid Mass Transfer in Three-Phase Fluidized Beds," *Int. Chem. Eng. Symp. Ser.*, No. 38, *Multiphase Flow Systems, I,* Inst. Chem. Engrs., London, Paper B2 (1974).

Leonard, J. H., and G. Houghton, "Mass Transfer and Velocity of Rise Phenomena for Single Bubbles," *Chem. Eng. Sci.*, **18,** 133 (1963).

Lochiel, A. C., and P. H. Calderbank, "Mass Transfer in the Continuous Phase around Axisymmetric Bodies of Revolution," *Chem. Eng. Sci.*, **19,** 471 (1964).

Mellon, M. G., *Analytical Absorption Spectroscopy,* Wiley, New York (1950).

Nguyen-Tien, K., A. N. Patwari, A. Schumpe, and W.-D. Deckwer, "Gas-Liquid Mass Transfer in Fluidized Particle Beds," *AIChE J.*, **31,** 194 (1985).

Ostergaard, K., and W. Suchozebrski, "Gas-Liquid Mass Transfer in Gas-Liquid Fluidized Beds," *Proc. 4th Eur. Symp. Chem. Reac. Eng.*, Pergamon, Oxford, 21 (1971).

Tsuchiya, K., and L.-S. Fan, "Near-Wake Structure of a Single Bubble in a Two-Dimensional Liquid-Solid Fluidized Bed: Vortex Shedding and Wake Size Variation," AIChE Ann. Meet. Miami Beach, Nov. 2–7, 1986; *Chem. Eng. Sci.*, **43,** 1167 (1988).

Tsuchiya, K., G. H. Song, and L.-S. Fan, "Effects of Particle Properties on Bubble Rise and Wake in a Two-Dimensional Liquid-Solid Fluidized Bed," *Chem. Eng. Sci.* (1989).

Vanderschuren, J., J. P. Schrayen, and S. Roland, "Etude du Transfert de Matiere Pendant L'ascension D'une Grosse Bulle Gazeuse Dans un Lit Fluidise Liquide," *Fluidization and Its Applications,* by H. Angelino et al., eds., Cepadues, Toulouse, 351 (1974).

Weber, M. E., "The Effect of Surface-Active Agents on Mass Transfer from Spherical-Cap Bubbles," *Chem. Eng. Sci.*, **30,** 1507 (1975).

Weller, K. R., "Mass Transfer from a Single Gas Bubble," *Can J. Chem. Eng.*, **50,** 49 (1972).

Wilke, C. R., and P. Chang, "Correlation of Diffusion Coefficients in Dilute Solutions," *AIChE J.*, **1,** 264 (1955).

Yabe, K., and D. Kunii, "Dispersion of Molecules Diffusing from a Gas Bubble into a Liquid," *Int. Chem. Eng.*, **18,**(4), 666 (1978).

Manuscript received June 14, 1989, and revision received Dec. 5, 1989.